Journal of Power Sources 250 (2014) 257–265

Contents lists available at ScienceDirect

Journal of Power Sources

journal homepage: www.elsevier.com/locate/jpowsour

# Phosphorous and nitrogen dual heteroatom doped mesoporous carbon synthesized via microwave method for supercapacitor application

Udaya B. Nasini [a], Venu Gopal Bairi [a], Sunil Kumar Ramasahayam [a], Shawn E. Bourdo [b], Tito Viswanathan [a,1], Ali U. Shaikh [a,*]

[a] Department of Chemistry, University of Arkansas at Little Rock, 2801 South University Ave, Little Rock, AR 72204, USA
[b] Center for Integrative Nanotechnology Sciences, University of Arkansas at Little Rock, 2801 South University Ave, AR 72204, USA

## HIGHLIGHTS

- Phosphorous, nitrogen doped carbon were synthesized by microwave technique.
- Evaluation of supercapacitor property toward supercapacitor application.
- Characterization and comparison of different doped carbon materials.
- Correlation of surface and physical characteristics on EDL and pseudocapacitance.
- Excellent electrocatalytic activity having high specific & interfacial capacitance.

## GRAPHICAL ABSTRACT

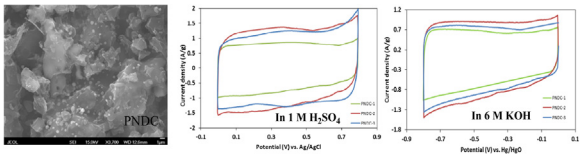


## ARTICLE INFO

*Article history:*
Received 11 May 2013
Received in revised form
2 October 2013
Accepted 11 November 2013
Available online 19 November 2013

*Keywords:*
Nitrogen and phosphorus mesoporous doped carbon
Specific capacitance
Pseudocapacitance
Interfacial capacitance
Supercapacitor

## ABSTRACT

Phosphorus (P) and nitrogen (N) dual heteroatom doped mesoporous carbon (PNDC) synthesized by microwave assisted carbonization of tannin cross-linked to melamine in the presence of polyphosphoric acid was evaluated electrochemically for supercapacitor application. Controlling the N content by varying the amount of tannin to melamine in the carbonization process produced varying nitrogen, phosphorus and oxygen functionalities along with different physical properties. Electrochemical characterization studies revealed that N content is responsible for pseudocapacitance and high surface area plays a vital role in improving the capacitative behavior by enhanced electric double layer formation. In 1.0 M $H_2SO_4$ and 6.0 M KOH, PNDC-2 showed a high specific capacitance of 271 F $g^{-1}$ and 236 F $g^{-1}$, respectively. XPS results demonstrate the presence of pyridinic–N, quaternary–N as well as quinone type oxygen functionalities, which accounts for redox reactions and likely play an important role in the transportation of electrons during the charge/discharge process. Thus, the microwave assisted synthesis of doped carbon can provide a novel method of synthesizing materials useful for the fabrication of cheap and high performance supercapacitors.



## 1. Introduction

Supercapacitors are one of the most promising energy storage devices useful for automobiles, electronics and energy systems. The advantage of supercapacitors is that they can be charged and

* Corresponding author. Tel.: +1 501 569 8837; fax: +1 501 569 8838.
*E-mail addresses:* txviswanatha@ualr.edu (T. Viswanathan), aushaikh@ualr.edu (A.U. Shaikh).
[1] Tel.: +1 501 569 8825; fax: +1 501 569 8838.

0378-7753/$ – see front matter © 2013 Elsevier B.V. All rights reserved.
http://dx.doi.org/10.1016/j.jpowsour.2013.11.014

discharged at high rates and can be coupled with fuel cells to deliver high energy in vehicles [1]. Electrical double layer capacitors (EDLCs) are very efficient in the storage and release of electrical energy. Electrostatic interactions between electrolyte ions and the electrode surface results in the generation and storage of energy [2–4]. Few metal oxides and conductive polymers also undergo Faradaic redox reactions to produce pseudocapacitance. However they are very expensive and have short cycling stability [4].

Capacitance of EDLC can be enhanced by improving the physicochemical properties of the two dimensional carbon materials, such as good conductivity, high surface area, pore size distribution and pore structure [3,5]. Although commercially available activated carbon (AC) and carbon nanotubes (CNTs) are very stable and have high power density [6–8], they are not efficient due to their limited electric double layer (EDL) capacitance that hinders ion transport through the micropores and thin pore walls [9–14].

Several types of carbon materials like activated carbon (AC) [7], carbon nanotubes (CNTs) [6], carbon onions [15], carbon nano fibers [16], and graphene [17–19] have been employed as electrode materials with good capacitative properties [20]. The capacitative behavior of these materials mainly depends on the type of the synthetic methods to achieve good surface area, porosity and highly ordered structures. Capacitance of the carbon material can be improved further by the introduction of pseudocapacitative property, which significantly enhances the interfacial capacitance ($C_i$). An extensive research on this type of carbon material indicates that the introduction of various functionalities with several hetero atoms like P, N, oxygen (O), sulfur, and boron could improve the electronic properties on the surface of the space charge layer [21–24].

Recent developments in doped carbon with dual-heteroatom doping showed superior pseudocapacitance due to the high electron donating property to proton and/or charge density enhancement of the carbon surface [25–28]. A detailed study of dual doping with two different elemental atoms offers a particular mechanistic way to study the influence of dual atoms on the electrochemical performance. Efforts to introduce heteroatoms with good electrochemical properties are important. So far, different synthetic techniques are employed to synthesize dual heteroatom doped carbon material from various organic sources. In this report, phosphorus nitrogen doped carbons (PNDCs) prepared by a microwave-assisted method were evaluated for their capacitative behavior and compared with the literature values of nonmetal doped carbon materials [29]. In this work, different versions of PNDCs were studied electrochemically. The synthetic procedure developed for preparing PNDCs involved 30 min of irradiation of precursor material. Modification of the carbon lattice with P and N changes the capacitance by changing the electric double layer capacitance and pseudocapacitance. Hence, this carbon material with excellent capacitance, cyclic stability and high power density can be useful in developing cheap and efficient EDLCs.

## 2. Experimental

Various N and P doped carbon materials (PNDC-1 with the highest N and P content, through PNDC-3 with the lowest N and P content) were synthesized by changing the proportion of melamine and hexamine (N source) to tannin (C source). The materials were added to hot water and stirred to get a homogeneous suspension. An aqueous solution of hexamine was added to the mixture with continuous heating and stirring. The resulting polymer was microwaved after mixing with polyphosphoric acid using a 1.25 kW and 2.4 GHz frequency microwave for 30 min. The detailed method of synthesis is reported elsewhere [30,31]. Polyphosphoric acid employed in the synthesis serves both as the source of P as well as a microwave absorber. The microwaving temperature was estimated to be between 1200 and 1400 °C during the carbonization process. The list of PNDCs is given in Table 1.

### 2.1. Physical characterization

The structural analysis and morphological studies were carried out by scanning electron microscopy (SEM, JEOL 7000). The elemental composition of these materials was determined by using a K-alpha X-ray photoelectron spectrometer (XPS) by Thermo Fisher Scientific Company. XPS data analysis was performed using Thermo Avantage software; all spectra were peak shifted to the C1s photoemission peak at 285.0 eV. Nitrogen sorption studies, surface area and pore size distribution were obtained by Brunauer–Emmett–Teller (BET) method on powdered samples at a bath temperature of 77.3 K using Micromeritics surface area analyzer (ASAP-2020).

## 3. Electrochemical measurements

Cyclic voltammetric evaluation was carried out at room temperature using a Pine Instruments (Raleigh, NC) bipotentiostat (Model AFCBP1) with a three electrode probe system. Galvanostatic measurements were performed using EG&G Instruments (Princeton Applied Research) bipotentiostat/Galvanostat Model 283. The electrochemical investigation of N and P modified carbon materials for supercapacitor application was carried out both in an alkaline medium (6.0 M KOH) as well as in an acid medium (1.0 M $H_2SO_4$). The test electrode was prepared by loading a slurry mixture containing the active material, carbon black and poly tetrafluoroethylene (PTFE) in a mass ratio of 90:5:5 on a glassy carbon electrode and dried under vacuum. The catalyst loading on the glassy carbon electrode was estimated to be about 0.51 mg $cm^{-2}$ area of the electrode. A platinum wire was used as the counter electrode, and an Hg/HgO electrode (in 6 M KOH) or an Ag/AgCl electrode (in 1 M $H_2SO_4$) was used as the reference electrode. The electrolyte solution was purged with nitrogen ($O_2$ free) for 30 min prior to electrochemical measurements. The cyclic voltammograms were obtained in the potential range of −1.0–0.0 V vs. Hg/HgO in 0.1 M KOH and 0.0–0.8 V vs. Ag/AgCl in 1 M $H_2SO_4$ at different scan rates ranging from 5 to 100 mV $s^{-1}$.

The specific capacitance ($C_s$) was calculated from the cyclic voltammograms and galvanostatic charge–discharge curves. From cyclic voltammograms, average values of the positive and negative sweep currents were used to calculate the $C_s$ by employing Equations (1) and (2), where i is the current density of the anodic and cathodic branches, $V$ is the potential, $v$ is the potential sweep rate and $m$ is the mass of the active material. From, the galvanostatic charge–discharge curves $C_s$ was calculated using Equation (1), where i is the applied current and $\Delta t$ is the discharge time. The chronopotentiograms were performed at a constant current in the voltage range of −1.0 and 0.0 V. The charge–discharge curves of all samples were obtained after two cycles to avoid the interference of oxygen on the electrode surface.

**Table 1**
Amounts of precursor materials utilized in the synthesis of PNDCs.

| Sample | Molar ratio Tannin:Melamine: Hexamine | Tannin, g | Melamine, g | Hexamine, g |
|---|---|---|---|---|
| PNDC-1 | 1:3:1 | 2.88 | 3.78 | 1.4 |
| PNDC-2 | 1:2:2/3 | 2.88 | 2.52 | 0.93 |
| PNDC-3 | 1:0.5:1/6 | 2.88 | 0.62 | 0.23 |

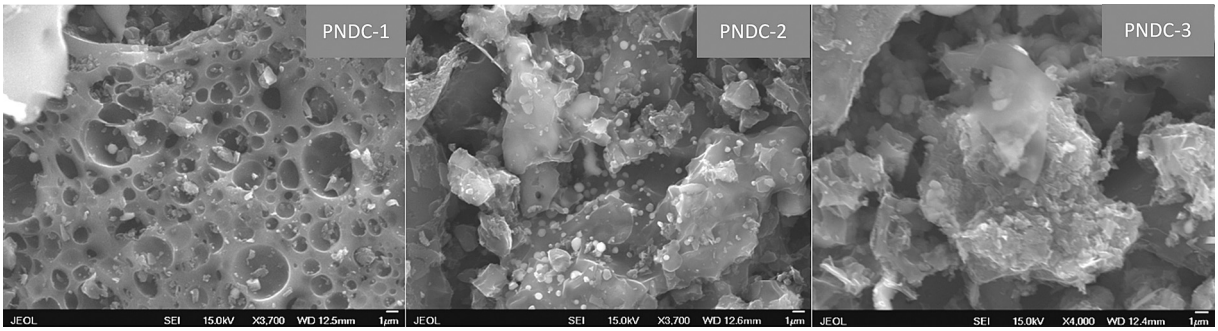


**Fig. 1.** Scanning electron microscopic images of PNDCs (scale bar 1 μm). a) PNDC-1, b) PNDC-2, and c) PNDC-3.

$$C_s = \int i(dV)/V.m.v = Q/\Delta V.m = \int idt/\Delta V.m = i\Delta t/\Delta V.m \quad (1)$$

$$C_{s,} = (C_{anode} + C_{cathode})/2 \quad (2)$$

The interfacial capacitance ($C_i$) can be calculated from $C_s$ and $S_{BET}$ (Brunauer–Emmett–Teller (BET)) surface area using Equation (3).

$$C_i = C_s/S_{BET} \quad (3)$$

The specific energy (SE) and the specific power (SP) of PNDCs were calculated from the galvanostatic charge–discharge curves and cyclic voltammograms using the Equations (4) and (5), respectively.

$$SE = \left(C_s.V^2\right)\Big/2 \times 3600 \quad (4)$$

$$SP = (SE/\Delta t) \times 3600 \quad (5)$$

## 4. Results and discussion

### 4.1. Morphological and physical characterization

The SEM images, as shown in Fig. 1a–c, exhibit the presence of porous carbon with spherical dopant particles incorporated along with some irregular surface structures. A dense formation of these spheres was observed with very rough surface. SEM images clearly show the growth of these spheres out of the plane of the carbon matrix. The PNDCs exhibit similar graphitic flakes as well as spherical surface morphologies. But PNDC-1 shows different surface with less flake surface due to high surface functionalities, and synthetic effect [30].

BET analysis was performed using nitrogen adsorption–desorption isotherms to determine the porous nature of the material. The surface area ($SA_{BET}$), average pore diameter ($D_{BJH}$), total pore volume ($V_{total}$), micropore volume ($V_{micro}$), mesopore volume ($V_{meso}$) and average pore width ($W_{BET}$) of all the composites are listed in Table 2.

The nitrogen adsorption–desorption isotherms of the PNDCs are shown in Fig. 2a, where the curves represent type IV isotherms with H2 hysteresis loop according to IUPAC classification [32,33]. Sharp capillary condensation can be observed in the relative pressure ($P/P_0$) range of 0.4–0.8, which indicate the presence of mesoporous diameter distribution with a narrow pore size of ~ 2–4 nm (Fig. 2b). A difference in the ratio of melamine and hexamine to tannin ratio resulted in varying surface area and porosity. According to BET analysis, PNDC-1 showed less porosity, when compared with the PNDC-2 and PNDC-3, due to melting and shrinking, thus significantly reducing the stability of PNDC-1 during microwave treatment. Therefore, gases released during this process could not form large number of mesopores as in the other two samples. PNDC-2 and PNDC-3 have shown decent mesopore volume and nitrogen adsorption–desorption curves. The BET surface area of the PNDC-1 with 9.7% nitrogen content produced only 113 $m^2\ g^{-1}$. The surface area increases significantly as the amount of melamine (nitrogen source) is reduced in the carbonization process. The PNDC-2 (1.5% nitrogen) and PNDC-3 (0.35% nitrogen) with high surface area of 479 $m^2\ g^{-1}$ 855 $m^2\ g^{-1}$ were achieved, respectively. A high amount of melamine incorporation has an impact on the reduced pore volume and surface area due to the formation of bulky polymer from melamine on the surface blocking the pores. PNDC-1, with the highest N content (9.7 atom%) has very low surface area and porosity (loss of mesopores and micropores) due to the lodging of excess N both on the surface sites as well as in pores [34,35].

The photoemission spectrum from a typical XPS survey scan is presented in Fig. 3, and the summary elemental analysis for all PNDCs is presented in Table 3. Survey scans and narrow scan spectra for the main elements of interest–nitrogen, phosphorous and oxygen–can also be found in the Supporting information for all PNDCs. After deconvolution of the peaks, several atomic environments were determined to exist. Based on the elemental analysis from the survey scan and the individual atomic environments from the narrow scan deconvolution, atomic percent were calculated for specific functionalities.

The narrow scan XPS analysis (Figs S1, S2 and S3, Supporting information) gives valuable insight into the functional groups present on the surface of the PNDCs. Specific functionalities are identified based on their binding energies and are listed in Table 4 along with atomic percentages. For nitrogen (Figs S1b, S2b, and S3b in Supporting information), photoemission peaks corresponding to

**Table 2**
BET analysis of PNDCs.

| Sample | $SA_{BET}$ surface area ($m^2\ g^{-1}$) | $D_{BJH}$ pore diameter (nm) | $V_{total}$ total pore volume ($cm^3\ g^{-1}$) | $V_{micro}$ micropore volume ($cm^3\ g^{-1}$) | $V_{meso}$ mesopore volume ($cm^3\ g^{-1}$) | $W_{BET}$ pore width (nm) |
|---|---|---|---|---|---|---|
| PNDC-1 | 113 | 4.44 | 0.103 | 0.0012 | 0.102 | 3.625 |
| PNDC-2 | 479 | 3.29 | 0.313 | 0.0685 | 0.244 | 2.610 |
| PNDC-3 | 855 | 4.07 | 0.650 | 0.0676 | 0.582 | 3.030 |

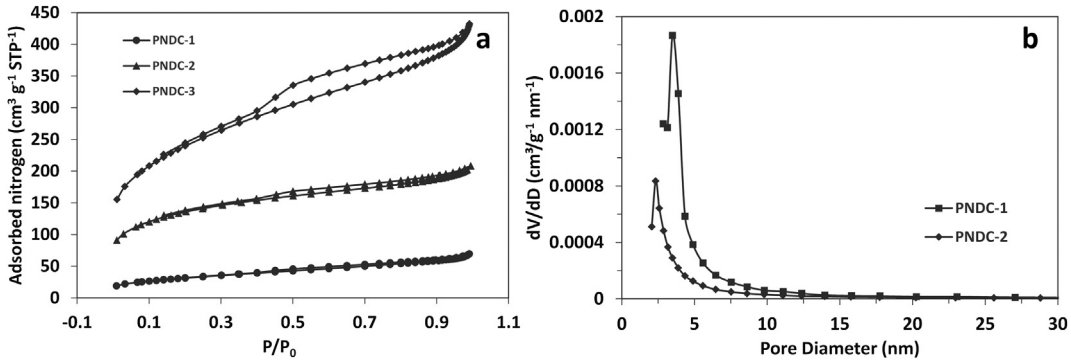


**Fig. 2.** a) Nitrogen sorption isotherms of PNDCs, b) Pore size distribution of PNDC-1 and PNDC-2.

pyrrolic/pyridonic nitrogen (N1, ~399.6 eV), pyridinic nitrogen (N2, ~398.5 eV), quaternary/graphitic nitrogen (N3, ~401.5 eV), and N–oxide (N4, >403 eV) have been observed [16,30,32,36–39]. The highest amount of pyridinic–N (3.0 atom %) was observed in PNDC-1, and the highest amount of quaternary–N (0.23 atom %) in PNDC-3. Three different types of phosphorus environments were determined to exist (Figs S1c, S2c, and S3c in Supporting information): P1 (134.1 eV, P=O), unknown higher energy levels of P2 (136.5 eV) and P3 (138.5 eV) were confirmed by deconvolution of the P2p photoemission peaks. Along with nitrogen and phosphorus, oxygen was also detected on the surface of the mesoporous carbon material.

XPS data revealed an interesting correlation between nitrogen and oxygen content in the carbons. This microwave carbonization technique, along with melamine treated samples, resulted in high nitrogen functionalities. This has been attributed to the difference in chemical interactions of precursors with oxygen containing functional groups and the overall mechanism of carbonization [34]. In this case, PNDC-1 and PNDC-2 exhibited high oxygen content (14.9% and 10%, respectively) when compared to PNDC-3 (Table 3). PNDC-1 and PNDC-2 exhibit higher oxygen content that has been attributed to the higher ratios of N1, N4, and P1 functionalities as shown in Table 4. Since PNDC-3 has less of these specific N- and P-functionalities, it also contains less oxygen. The photoemission peaks from the O1s narrow scans (Figs S1d, S2d, and S3d in Supporting information) reveal the existence of four types of oxygen functionalities at binding energies of ~531eV (O1, quinone), ~533 eV (O2, carbonyl), ~535eV (O3, C–O–C), and ~537.5 eV (O4, chemisorbed oxygen of carboxylic or water). Among these four oxygen functionalities, quinone groups in the carbon matrix are responsible for the pseudocapacitance involving redox reactions [40]. Data from literature and XPS analysis can be applied to explain the capacitative performance of the PNDCs. The effect of nitrogen and oxygen content, surface area and porosity of the PNDCs on the capacitance is further evaluated by electrochemical characterization. It will be seen that the quinine groups of PNDC-1 and PNDC-2 are critical to pseudocapacitative behavior.

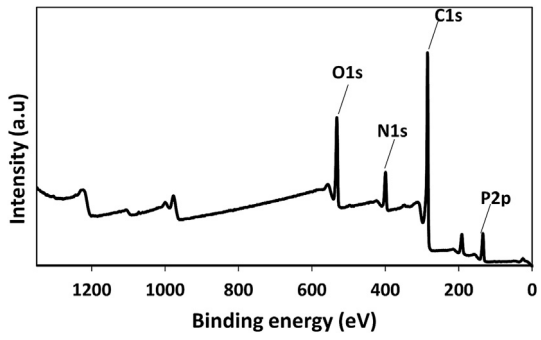


**Fig. 3.** XPS survey scan spectra of PNDC-1.

### 4.2. Electrochemical characterization

#### 4.2.1. Electrochemical studies in 1 M sulfuric acid

The cyclic voltammograms of PNDC samples obtained at the scan rate of 5 mV $s^{-1}$ in 1 M $H_2SO_4$ electrolyte with an Ag/AgCl reference electrode are shown in Fig. 4a. A comparative study of all PNDCs established a clear relationship of surface functionalities and material properties in the formation of electric double layer and pseudocapacitance. All three PNDCs exhibited almost a perfect rectangular shape signifying a double layer capacitance behavior, which can be accounted for by a high surface area, porosity, and nitrogen/oxygen content. Even at high scan rates (100 mV $s^{-1}$) the shape of the voltammogram looks similar (Fig. 4b). A maximum current density was observed at ca. 0.4 V, and an almost constant current response was observed in the potential range of 0.5 to 0.1 V (vs. Ag/AgCl). The highest $C_s$ for synthesized PNDC-1, PNDC-2 and PNDC-3 in 1 M $H_2SO_4$ were172 F $g^{-1}$, 272 F $g^{-1}$ and 246 F $g^{-1}$, respectively. These capacitance values are higher than those

**Table 3**
Results of N1s, P2p, C1s and O1s core level XPS spectra of PNDCs.

| Sample | C 1s (At %) | N 1s (At %) | P 2p (At %) | O 1s (At %) |
|---|---|---|---|---|
| PNDC-1 | 66.4 | 9.7 | 9.0 | 14.9 |
| PNDC-2 | 85.4 | 1.5 | 3.0 | 10.0 |
| PNDC-3 | 94.6 | 0.35 | 0.6 | 4.4 |

**Table 4**
Detailed XPS analysis of PNDCs: calculated N, P, – doping and oxygen types (atom%).

| Element ID, functionality | PNDC-1 | PNDC-2 | PNDC-3 |
|---|---|---|---|
| N1, pyrrolic/pyridonic | 1.9% (399.6 eV) | – | – |
| N2, pyridinic | 3.0% (398.4 eV) | 0.20% (398.8 eV) | 0.05% (398.3 eV) |
| N3, quaternary/graphitic | 3.6% (401.2 eV) | 1.0% (401.5 eV) | 0.23% (401.9 eV) |
| N4, N – oxide | 1.2% (403.1 eV) | 0.3% (405.5 eV) | 0.07% (406.0 eV) |
| P1, phosphonyl | 6.0% (134.1 eV) | 2.5% (134.2 eV) | 0.23% (135.0 eV) |
| P2, unassigned | 2.1% (136.5 eV) | 0.3% (137.2 eV) | 0.32% (137.4 eV) |
| P3, unassigned | 0.9% (138.5 eV) | 0.2% (139.4 eV) | 0.05% (141.0 eV) |
| O1, quinone | 3.6% (531.0 eV) | 1.8% (531.1 eV) | – |
| O2, carbonyl | 7.3% (532.8 eV) | 6.4% (532.9 eV) | 1.7% (532.9 eV) |
| O3, ether | 3.3% (535.0 eV) | 1.3% (535.3 eV) | 2.2% (535.0 eV) |
| O4, chemisorbed oxygen | 0.7% (537.5 eV) | 0.5% (537.8 eV) | 0.5% (537.3 eV) |

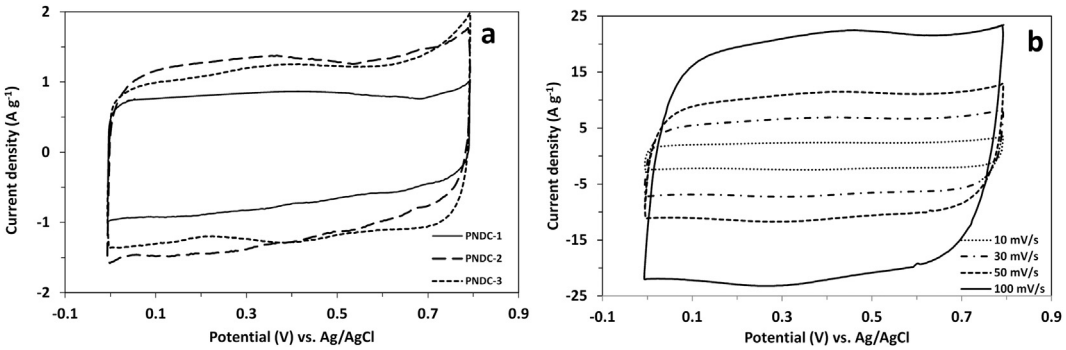


**Fig. 4.** Cyclic voltammetry plots of PNDCs in 1 M $H_2SO_4$, a) recorded at a sweep rate of 5 mV $s^{-1}$ and b) PNDC-2 at different scan rates.

reported earlier for N-doped carbon based materials [32,38]. This tremendous response of the PNDCs can be attributed to the combined electric double layer capacitance and pseudocapacitative behavior. PNDC-2 has the highest specific capacitance in 1 M $H_2SO_4$. From the cyclic voltammetric measurements (Fig. 4), PNDC-2 at potential range of 0–0.4 V (vs. Ag/AgCl) shows higher current density, indicating redox reaction associated with pyridinic nitrogen (0.20 atom%) and high quinone oxygen content (1.8 atom%), compared to that of PNDC-3 (0.05 atom% of pyridinic nitrogen and no quinone type of oxygen). However; PNDC-3 at potentials more positive than 0.6 V (vs. Ag/AgCl) has similar current density, which could be due to enhanced electric double layer in relation to high surface area of the material (855 $m^2$ $g^{-1}$). PNDC-1 has shown low capacitance value, most likely due to low pore volume (Fig. 2a) even though it has high pyridinic nitrogen (3.0 atom%) and quinone oxygen (3.6 atom%).

It is very important to have suitable pore size, pore volume, surface area and surface functionalities which can improve the EDL and pseudocapacitance [5,11,16]. The $C_s$ of the carbon material can be influenced by the pore size and pore volume. The presence of nitrogen species and high mesoporous volume in the PNDCs facilitates the ion transportation and penetration into the carbon matrix. Thus the wettability of the electrode surface improves with low diffusion resistance [27,41]. All the PNDC samples have similar pore size of ~3 nm and suitable for the accessibility of electrolyte ions to the interior surface of the porous carbon, which can improve the formation of EDL and the occurrence of corresponding redox reactions [42]. The adsorption–desorption isotherms of all the PNDCs have a similar shape but the amount of the nitrogen adsorbed is low in PNDC-1. Consequently, the BET surface area of the PNDC-1 drastically decreased due to low porosity and high surface functionalities. Hence, PNDC-1 shows low $C_s$ in which pseudocapacitance from redox reactions of nitrogen and oxygen functionalities play substantial role towards the total capacitance.

The pseudocapacitative behavior is due to the redox reactions involved between the electrolyte ions and the doped functionalities on the surface of the electrode material [13,43]. These reactions account for the pseudocapacitance of the material depending on the electrolyte and its pH conditions. Faradaic reactions that occur in acidic electrolyte involve nitrogen and oxygen functionalities [35,39]. In acidic environment, quinone type reactions are dominant redox reactions (as shown in Equation (6)) for pseudocapacitance that contribute to total capacitance [21,40]. Apart from these nitrogen reactions pyridone and pyridinic type nitrogen provides pseudocapacitance through redox reactions involving protons as shown in Equation (7) and (8), respectively. Based on the above results, a clear mechanistic understanding of pseudocapacitance contribution from the oxygen and nitrogen functionalities was established. The Faradaic reactions responsible for pseudocapacitance are shown below:

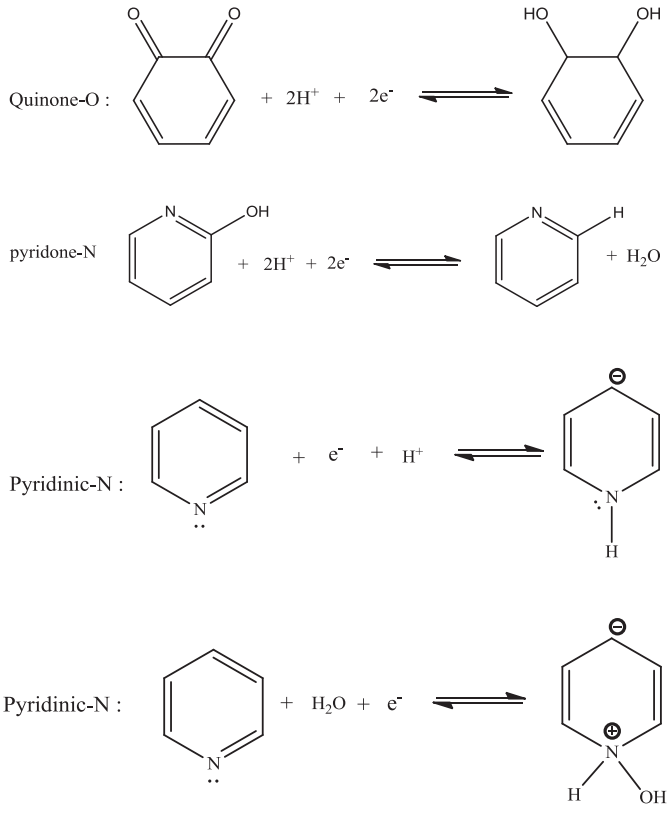


In acidic electrolyte, the presence of nitrogen functional groups is not only responsible for pseudocapacitance but they also enhance the electric double layer capacitance The surface charge of the carbon material due to the presence of more basic nitrogen environments enhances the adsorption of acidic electrolyte [44]. The PNDCs with high pyridinic–N and pyridone forms of N increased the pseudocapacitance by electrochemical redox reactions. As we have observed from XPS analysis, PNDC-2 with pyridinic–N (2.0 atom %), quinone–O (1.8 atom%) and graphitic–N type (1.0 atom%) are responsible for high capacitance of 272 F $g^{-1}$(combination of pseudocapacitance and EDL). In case of PNDC-3, however, the absence of quinone–O, low N (0.35 atom %) and high quaternary–N (0.23 atom%) is responsible for low pseudocapacitance and high EDL capacitance ($C_s$ of 246 F $g^{-1}$)

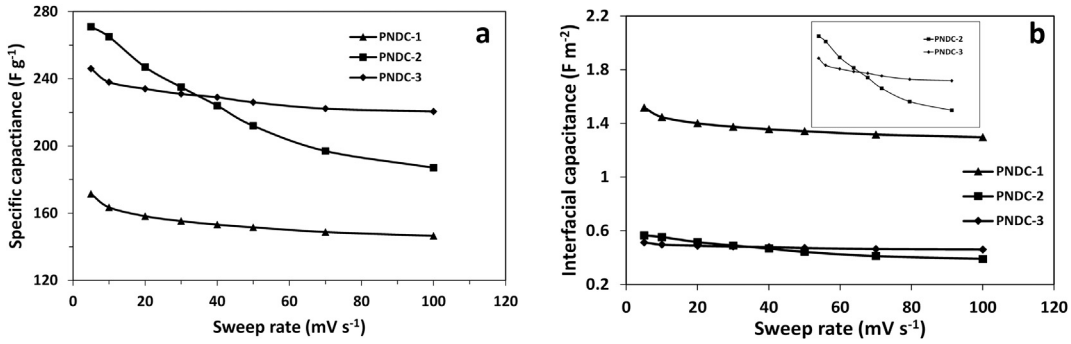


**Fig. 5.** Dependence of the specific capacitance and interfacial capacitance on the potential sweep rate from 5 to 100 mV $s^{-1}$ in 1 M $H_2SO_4$ (a, b).

by superior electron transport and conductive property of the material [27].

The capacitance per unit surface area, known as interfacial capacitance ($C_i$), depends on the pseudocapacitance of the material, which is directly proportional to the amount of N and O content. It is apparent that PNDC-1 with the highest N (9.7 atom%), O (14.9 atom%) content and low surface area (113 $m^2$ $g^{-1}$) accounted for the highest $C_i$ of 1.52 F $cm^{-2}$ and PNDC-3 with the highest surface area (855 $m^2$ $g^{-1}$) and lowest N (0.35 atom%), O (4.4 atom%) content resulted in 0.29 F $cm^{-2}$. But commonly available activated carbon has the $C_i$ of around 0.10–0.20 F $cm^{-2}$. This phenomenon of low surface area with high nitrogen content and high interfacial capacitance indicates the domination of pseudocapacitance. Likewise, a decrease in interfacial capacitance is due to increased double layer capacitance along with increased surface area. The increased availability of the surface doped nitrogen and oxygen environment in the carbon matrix with high electron donor–acceptor interactions results in improved pseudocapacitative behavior [32,45]. The interfacial capacitance also depends on the accessibility of mesopores and micropores to the electrolyte [38,46]. PNDC-1 with low surface area showed high interfacial capacitance according to the Equation (3). The greater adsorption of electrolyte ions results in high interfacial capacitance (capacitance per unit surface area). The other two PNDCs with large surface area and similar pore size, low nitrogen and oxygen functionalities clearly show low $C_i$ values. In conclusion, highly accessible surface area and the additional pseudocapacitance contribution of the nitrogen and oxygen containing functionalities are responsible for high capacitance [45–48].

In order to establish the relative contribution of pseudocapacitance and double layer capacitance toward the total capacitance of each PNDC, measurements were conducted at varying sweep rates (5–100 mV $s^{-1}$). As shown in Fig. 5, specific and interfacial capacitance of individual PNDC was plotted against the sweep rate. The $C_s$ values of the all PNDCs clearly show that an increase in sweep rate decreases the capacitance value. At low sweep rates, ions are accessible at the surface of the electrode material where high electric double layer and electrochemical kinetic redox reactions (pseudocapacitance) are possible [21,38]. At higher scan rates, all the PNDCs have shown a decrease in the $C_s$ due to less contribution from the EDL and redox reactions. It is very clear that PNDC-2 with more accessible surface area and high concentration of functionalities resulted in a drastic decrease in the $C_s$ (about ~ 30% loss in capacitance) which could be due to more redox based charge generation in between the electrode and electrolyte interface. In comparison, PNDC-3 with low N, O and very high surface area, demonstrated a high capacitance and most of it is due to EDL formation. As we increase the scan rate, a very small capacitance loss (~12%) was observed (Fig. 5a). These results suggest that high capacitance was observed from the PNDCs with high N content due to the contribution from pseudocapacitance when compared to very low N containing PNDC-3. The PNDCs exhibited low surface area and N content, yet high specific and interfacial capacitances were observed similarly to previously reported mesoporous doped carbons [48]. However, the $C_i$ of the PNDCs (Fig. 5b) is completely different when compared to the $C_s$. The nitrogen adsorption isotherms from BET analysis demonstrates that PNDC-1 with low porosity (surface area of 113 $m^2$ $g^{-1}$) and high N content (8.31 atom %) showed a very high $C_i$ value of 1.52 F $cm^{-2}$ compared to other doped carbon [49–51] and activated carbon materials [52]. In terms of $C_i$, high pseudocapacitance was due to high nitrogen in PNDC-1 (per unit surface area) shows a radical drop. A summary of $C_s$ and $C_i$ measurements in 1 M $H_2SO_4$ is presented in Table 5.

**Table 5**
Specific capacitance ($C_s$) and interfacial capacitances ($C_i$) of all PNDCs in 1 M $H_2SO_4$ and 6 M KOH.

| Sample | $C_s$ (1.0 M $H_2SO_4$) (F $g^{-1}$) | $C_i$ (1.0 M $H_2SO_4$) (F $cm^{-2}$) | $C_s$ (6.0 M KOH) (F $g^{-1}$) | $C_i$ (6.0 M KOH) (F $cm^{-2}$) |
|---|---|---|---|---|
| PNDC-1 | 172 | 1.52 | 176 | 1.55 |
| PNDC-2 | 272 | 0.58 | 236 | 0.50 |
| PNDC-3 | 246 | 0.29 | 187 | 0.22 |

### 4.2.2. *Electrochemical studies in 6 M potassium hydroxide*

In a proton free alkaline electrolyte solution, the $C_s$ and $C_i$ measurements were recorded using Hg/HgO reference electrode. Even at high scan rates, the PNDCs show almost a rectangular shape similar to that of in acidic electrolyte (Fig. 6a and b). In contrast, the voltammograms of PNDCs have not shown redox wave generated by oxygen species. This observation validates that in alkaline medium the absence of pseudocapacitance is due to the electrochemically inactive quinone type (O1) oxygen functional groups [40]. The same trend was followed by PNDCs in 6 M KOH as in 1 M $H_2SO_4$, but the specific capacitance values obtained were smaller in alkaline electrolyte. The specific capacitances of PNDC-1, PNDC-2 and PNDC-3 are 236 F $g^{-1}$, 176 F $g^{-1}$ and 186 F $g^{-1}$; respectively. PNDC-2 with 0.20 atom% N2, 1.0 atom % N3 and surface area of 479 $m^2$ $g^{-1}$ has the highest $C_s$ of in 6 M KOH. The PNDC-3 with low N2 (0.05 atom%) showed high capacitance in comparison to PNDC-1 (3.0 atom% of N2). This is due to the fact that highest surface area of 855 $m^2$ $g^{-1}$ and high mesopore volume enhancing the interaction of N atoms and electrolyte ions of $K^+$ in the solution, which leads to abundant number of $K^+$ ions on the electrode surface and thereby forming an electric double layer. In alkaline electrolyte, quinone type reactions are not possible to have pseudocapacitative redox reactions and the only possible reactions in alkaline electrolyte involving pyridinic nitrogen (N2) redox

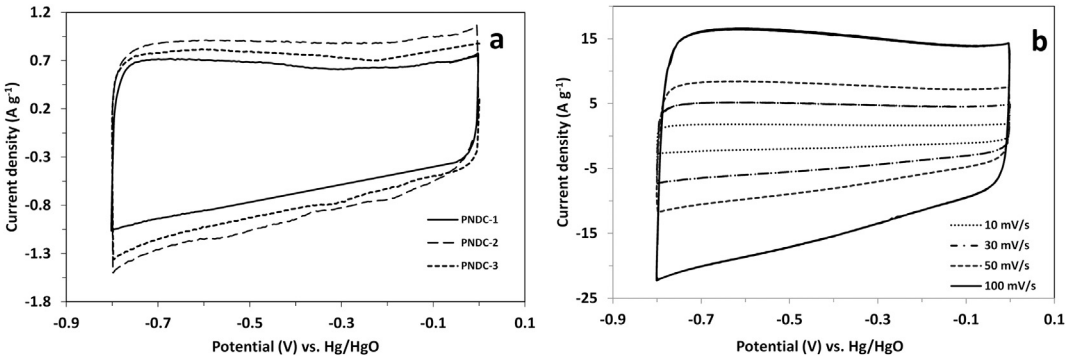


**Fig. 6.** Cyclic voltammetry plots of PNDCs in 6 M KOH a) recorded at a sweep rate of 5 mV $s^{-1}$ and b) PNDC-2 at different scan rates.

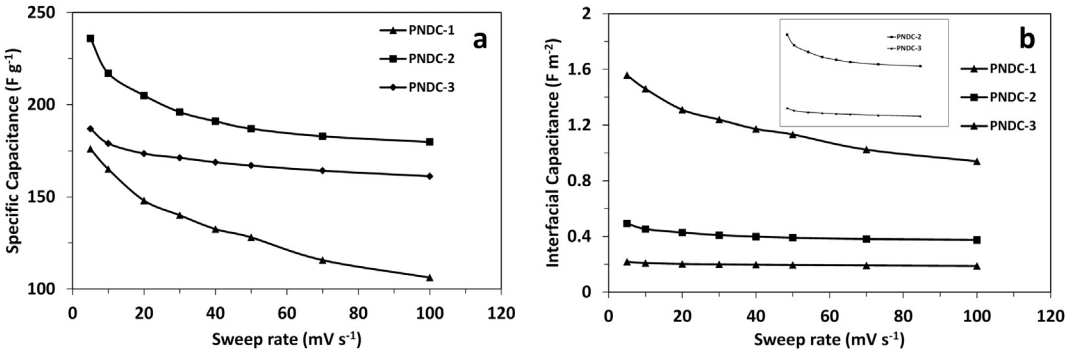


**Fig. 7.** Dependence of the specific capacitance and interfacial capacitance on the potential sweep rate from 5 to 100 mV $s^{-1}$ in 6 M KOH (a, b).

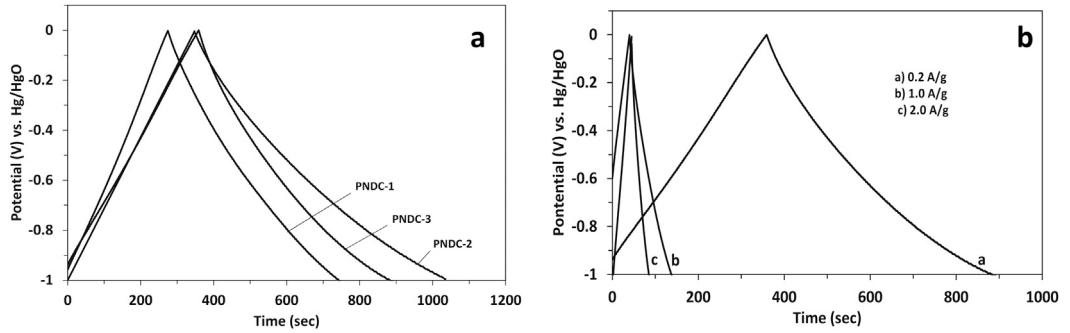


**Fig. 8.** Galvanostatic characterization of PNDCs a) charge–discharge curves of PNDCs at current density of 0.2 A $g^{-1}$, b) charge–discharge curves of PNDC-2 at different current densities.

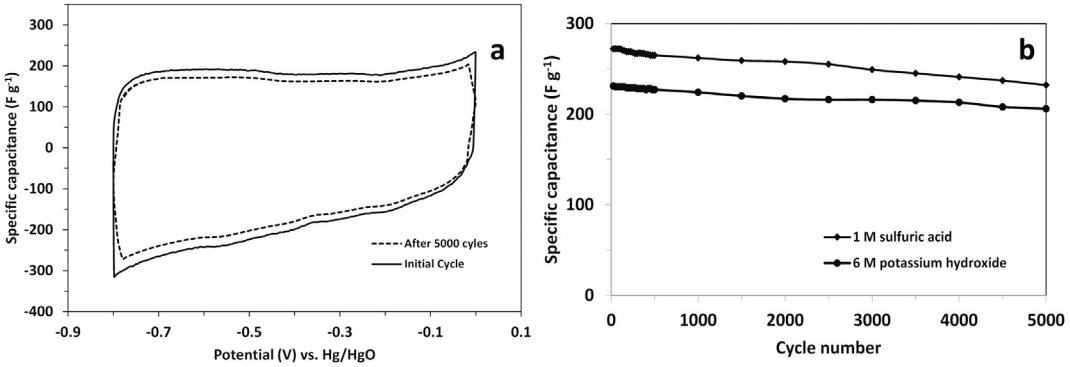


**Fig. 9.** Specific capacitance of PNDC-2 a) CV after first cycle and after 5000 cycles in 6 M KOH b) Specific capacitance vs. cycle number in acidic and alkaline electrolyte solutions.

**Table 6**
Specific energy and specific power of PNDCs in 1 M $H_2SO_4$.

| Sample | Specific energy (W h $kg^{-1}$) | Specific power (W $kg^{-1}$) |
|---|---|---|
| PNDC-1 | 26.3 | 201.5 |
| PNDC-2 | 38.2 | 204.6 |
| PNDC-3 | 29.2 | 200.6 |

reactions [40] (Equation (9)). From Fig. 7a, the specific capacitance drop of PNDC-1 and PNDC-2 is much higher indicating the pseudocapacitative redox reaction contribution. Similarly, interfacial capacitance drop (Fig. 7b) also signifies that pseudocapacitance (per surface area) is much higher in PNDC-1 followed by PNDC-2. The $C_s$ and $C_i$ values of the PNDCs in 6 M KOH are summarized in Table 5.

*4.2.3. Galvanostatic charge–discharge studies*

Further evaluation of the electrochemical performance of the PNDCs was performed by galvanostatic charge–discharge curves which illustrate the pseudocapacitance as well as the resistance of the material. Fig. 8a shows the galvanostatic charge–discharge curves of PNDCs with an applied current density of 0.2 A $g^{-1}$, Fig. 8b shows PNDC-3 at different current densities. All discharge curves of the PNDCs signify a distinct arc shape with an IR drop due to the low conductivity of the sample. PNDC-2 exhibited highest discharging slope and $C_s$, which can be attributed to its high surface area, porosity and N, P and O content [53]. Even at high current densities, PNDC-2 and PNDC-3 retained capacitance with only a trivial capacitance loss. This observation illustrates that the increased conductivity of PNDC-3 is by the virtue of quaternary N and low contribution of pseudocapacitance at high current density. The cyclic voltammetry measurements with a rectangular shape and little polarization at higher scan rates also proved the tremendous rate performance of the material. The cycling electrochemical stability was investigated from the CV curves of PNDC-2 at scan rates of 5 mV $s^{-1}$. Even after ~5000 cycles it showed a rectangular shape with a slight capacitance loss of 14.2% (Fig. 9) and in the case of PNDC-3 only an 11.6% capacitance loss was observed (not shown in figure). This shows that the PNDCs synthesized by this novel approach have excellent durability for practical applications. The specific energy (SE) and specific power (SP) were calculated from galvanostatic charge–discharge curves using Equations (4) and (5). Table 6 shows the calculated SE and SP of the PNDCs in 1 M $H_2SO_4$ electrolyte solution. Higher SE was obtained for the PNDCs which is attributed to a high pseudocapacitance due to the doping of N and P in the carbon matrix. In addition, dual doping of N along with P shows high capacitative behavior even at higher scan rates or current densities due to the stabilizing capacity of N and P as dopants. P doping of carbon material is known to improve the electronic properties and stability of the material [24,37].

## 5. Conclusions

A new microwave technique has been used to synthesize nitrogen, phosphorous and oxygen enriched mesoporous carbon materials for supercapacitor properties. By varying the concentration of melamine as nitrogen dopant, several surface functionalities and structural differences were observed. An effect of these parameters towards supercapacitor application was studied in 1 M $H_2SO_4$ and 6 M KOH. The PNDC-2 with high pyridinic–N, quinone–O, high surface area, pore size and pore volume showed excellent electrochemical performance specific capacitance in both acidic (272 F $g^{-1}$) and alkaline media (246 F $g^{-1}$). High nitrogen doping of PNDC influenced the surface characteristics by generating low surface area with low $C_s$ and high $C_i$. The contribution of pseudocapacitance and double layer capacitance with respect to redox reactions and other physical characteristics was evaluated. All the PNDCs have tremendous capacitance, stability, and cycleability. Therefore, PNDCs prepared from renewable sources via microwave technique with varying N content could be promising candidates for supercapacitors in both acidic and alkaline electrolyte.

## Acknowledgments

We are grateful for the help in the characterization studies by Center for Integrative Nanotechnology Sciences, University of Arkansas at Little Rock.

## Appendix A. Supplementary data

Supplementary data related to this article can be found at http://dx.doi.org/10.1016/j.jpowsour.2013.11.014.

## References

[1] H. Zhao, A.F. Burke, in: Institute of Transportation Studies, University of California, Davis, 2010.
[2] B.E. Conway, Electrochemical Supercapacitors: Scientific Fundamentals and Technological Applications, Plenum Publishers, New York, 1999.
[3] E. Frackowiak, F. Beguin, Carbon 39 (2001) 937–950.
[4] J.P. Zheng, P.J. Cygan, T.R. Jow, J. Electrochem. Soc. 142 (1995) 2699–2703.
[5] M. Jayalakshmi, K. Balasubramanian, Int. J. Electrochem. Sci. 3 (2008) 1196–1217.
[6] H. Zhang, G. Cao, Y. Yang, Energy Environ. Sci. 2 (2009) 932–943.
[7] Y. Zhai, Y. Dou, D. Zhao, P.F. Fulvio, R.T. Mayes, S. Dai, Adv. Mater. 23 (2011) 4828–4850.
[8] H. Zhu, X. Wang, F. Yang, X. Yang, Adv. Mater. 23 (2011) 2745–2748.
[9] S.W. Lee, B.-S. Kim, S. Chen, Y. Shao-Horn, P.T. Hammond, J. Am. Chem. Soc. 131 (2008) 671–679.
[10] L.L. Zhang, X.S. Zhao, Chem. Soc. Rev. 38 (2009) 2520–2531.
[11] J. Chmiola, G. Yushin, R. Dash, Y. Gogotsi, J. Power Sources 158 (2006) 765–772.
[12] O. Barbieri, M. Hahn, A. Herzog, R. Kötz, Carbon 43 (2005) 1303–1310.
[13] P. Simon, Y. Gogotsi, Nat. Mater. 7 (2008) 845–854.
[14] A.G. Pandolfo, A.F. Hollenkamp, J. Power Sources 157 (2006) 11–27.
[15] D. Pech, M. Brunet, H. Durou, P. Huang, V. Mochalin, Y. Gogotsi, P.-L. Taberna, P. Simon, Nat. Nano 5 (2010) 651–654.
[16] L.-F. Chen, X.-D. Zhang, H.-W. Liang, M. Kong, Q.-F. Guan, P. Chen, Z.-Y. Wu, S.-H. Yu, ACS Nano 6 (2012) 7092–7102.
[17] Y. Shao, S. Zhang, M.H. Engelhard, G. Li, G. Shao, Y. Wang, J. Liu, I.A. Aksay, Y. Lin, J. Mater. Chem. 20 (2010) 7491–7496.
[18] H.M. Jeong, J.W. Lee, W.H. Shin, Y.J. Choi, H.J. Shin, J.K. Kang, J.W. Choi, Nano Lett. 11 (2011) 2472–2477.
[19] G. Zhao, T. Wen, C. Chen, X. Wang, RSC Adv. 2 (2012) 9286–9303.
[20] K.H. An, W.S. Kim, Y.S. Park, J.M. Moon, D.J. Bae, S.C. Lim, Y.S. Lee, Y.H. Lee, Adv. Funct. Mater. 11 (2001) 387–392.
[21] D.-w. Wang, F. Li, M. Liu, H.-m. Cheng, New Carbon Mater. 22 (2007) 307–314.
[22] H. Li, H.a. Xi, S. Zhu, Z. Wen, R. Wang, Microporous Mesoporous Mater. 96 (2006) 357–362.
[23] Y.J. Kim, Y. Abe, T. Yanagiura, K.C. Park, M. Shimizu, T. Iwazaki, S. Nakagawa, M. Endo, M.S. Dresselhaus, Carbon 45 (2007) 2116–2125.
[24] X. Zhao, A. Wang, T. Zhang, Preparation Method of Super Capacitor Electrode Material, CN Patent CN102013335 A, Apr 13, 2011.
[25] M. Kodama, J. Yamashita, Y. Soneda, H. Hatori, K. Kamegawa, Carbon 45 (2007) 1105–1107.
[26] E. Raymundo-Piñero, F. Leroux, F. Béguin, Adv. Mater. 18 (2006) 1877–1882.
[27] L. Sun, L. Wang, C. Tian, T. Tan, Y. Xie, K. Shi, M. Li, H. Fu, RSC Adv. 2 (2012) 4498–4506.
[28] X. Zhao, A. Wang, J. Yan, G. Sun, L. Sun, T. Zhang, Chem. Mater. 22 (2010) 5463–5473.
[29] G. Lota, K. Lota, E. Frackowiak, Electrochem. Commun. 9 (2007) 1828–1832.
[30] V. Bairi, S.E. Bourdo, U.B. Nasini, S. Ramasahayam, F. Watanabe, B.C. Berry, T. Viswanathan, Sci. Adv. Mater. 5 (2013) 1275–1281.
[31] U.B. Nasini, V. Gopal Bairi, S. Kumar Ramasahayam, S.E. Bourdo, T. Viswanathan, A.U. Shaikh, Chemelectrochem (2013), http://dx.doi.org/10.1002/celc.201300047.
[32] D.-W. Wang, F. Li, Z.-G. Chen, G.Q. Lu, H.-M. Cheng, Chem. Mater. 20 (2008) 7195–7200.
[33] C. Liu, Z. Yu, D. Neff, A. Zhamu, B.Z. Jang, Nano Lett. 10 (2010) 4863–4868.
[34] C. Devallencourt, J.M. Saiter, A. Fafet, E. Ubrich, Thermochim. Acta 259 (1995) 143–151.

[35] D. Hulicova-Jurcakova, M. Seredych, G.Q. Lu, T.J. Bandosz, Adv. Funct. Mater. 19 (2009) 438–447.
[36] J. Wei, D. Zhou, Z. Sun, Y. Deng, Y. Xia, D. Zhao, Adv. Funct. Mater. 23 (2013) 2322–2328.
[37] D. Hulicova-Jurcakova, M. Seredych, G.Q. Lu, N.K.A.C. Kodiweera, P.E. Stallworth, S. Greenbaum, T.J. Bandosz, Carbon 47 (2009) 1576–1584.
[38] D.-W. Wang, F. Li, Z.-S. Wu, W. Ren, H.-M. Cheng, Electrochem. Commun. 11 (2009) 1729–1732.
[39] Y.-H. Lee, K.-H. Chang, C.-C. Hu, J. Power Sources 227 (2013) 300–308.
[40] H.A. Andreas, B.E. Conway, Electrochim. Acta 51 (2006) 6510–6520.
[41] S.L. Candelaria, B.B. Garcia, D. Liu, G. Cao, J. Mater. Chem. 22 (2012) 9884–9889.
[42] D. Qu, H. Shi, J. Power Sources 74 (1998) 99–107.
[43] M. Seredych, M. Koscinski, M. Sliwinska-Bartkowiak, T.J. Bandosz, ACS Sustainable Chem. Eng. 1 (2013) 1024–1032.
[44] M.A. Montes-Morán, D. Suárez, J.A. Menéndez, E. Fuente, Carbon 42 (2004) 1219–1225.
[45] D. Hulicova, J. Yamashita, Y. Soneda, H. Hatori, M. Kodama, Chem. Mater. 17 (2005) 1241–1247.
[46] D. Hulicova-Jurcakova, M. Kodama, S. Shiraishi, H. Hatori, Z.H. Zhu, G.Q. Lu, Adv. Funct. Mater. 19 (2009) 1800–1809.
[47] S. Yoon, J. Lee, T. Hyeon, S.M. Oh, J. Electrochem. Soc. 147 (2000) 2507–2512.
[48] B. Xu, H. Duan, M. Chu, G. Cao, Y. Yang, J. Mater. Chem. A 1 (2013) 4565–4570.
[49] B. Xu, F. Wu, R. Chen, G. Cao, S. Chen, Y. Yang, J. Power Sources 195 (2010) 2118–2124.
[50] F. Meng, X. Zhang, B. Xu, S. Yue, H. Guo, Y. Luo, J. Mater. Chem. 21 (2011) 18537–18539.
[51] H.-J. Liu, J. Wang, C.-X. Wang, Y.-Y. Xia, Adv. Energy Mater. 1 (2011) 1101–1108.
[52] E. Frackowiak, Phys. Chem. Chem. Phys. 9 (2007) 1774–1785.
[53] C. Ma, J. Shi, Y. Song, D. Zhang, X. Zhai, M. Zhong, Q. Guo, L. Liu, Int. J. Electrochem. Sci. 7 (2012) 7587–7599.